

Pattern recognition system for the discrimination of multiple sclerosis from cerebral microangiopathy lesions based on texture analysis of magnetic resonance images

Pantelis Theodorakis^{a,*}, Dimitris Glotsos^b, Ioannis Kalatzis^b, Spiros Kostopoulos^a,
Pantelis Georgiadis^a, Koralia Sifaki^c, Katerina Tsakouridou^d, Menelaos Malamas^d,
George Delibasis^c, Dionisis Cavouras^b, George Nikiforidis^a

^aDepartment of Medical Physics, Medical Image Processing and Analysis Laboratory, University of Patras, 26500 Rio-Patras, Greece

^bDepartment of Medical Instruments Technology, Technological Educational Institute of Athens, Aigaleo, 12210 Athens, Greece

^cDepartment of MRI, 251 General Airforce Hospital, 11525 Athens, Greece

^dDepartment of MRI, Medical Diagnostic Center of Athens, 12131 Athens, Greece

Received 23 April 2008; revised 17 June 2008; accepted 24 July 2008

Abstract

In this study, a pattern recognition system has been developed for the discrimination of multiple sclerosis (MS) from cerebral microangiopathy (CM) lesions based on computer-assisted texture analysis of magnetic resonance images. Twenty-three textural features were calculated from MS and CM regions of interest, delineated by experienced radiologists on fluid attenuated inversion recovery images and obtained from 11 patients diagnosed with clinically definite MS and from 18 patients diagnosed with clinically definite CM. The probabilistic neural network classifier was used to construct the proposed pattern recognition system and the generalization of the system to unseen data was evaluated using an external cross validation process. According to the findings of the present study, statistically significant differences exist in the values of the textural features between CM and MS: MS regions were darker, of higher contrast, less homogeneous and rougher as compared to CM.

© 2009 Elsevier Inc. All rights reserved.

Keywords: Multiple sclerosis; Cerebral microangiopathy; Probabilistic neural network; Differential diagnosis

1. Introduction

Multiple sclerosis (MS) is a demyelinating disease of the central nervous system (CNS) which is characterized by a gradual loss of the myelin [1]. Its diagnosis is based primarily on clinical signs and symptoms; several para-clinical tests can help in its verification, while final decision is made by the neurologist. These tests include lumbar puncture, oligoclonal banding, visual and/or auditory evoked potentials, and magnetic resonance imaging (MRI) [2].

When the clinical signs and symptoms do not fulfill the diagnostic criteria of MS, MRI evaluation is needed in order to support dissemination in space and/or time [3]. The radiologist's diagnosis is based on MS imaging characteristics as depicted on MR images. These include ovoid and hyperintense lesions on T2-weighted (T2-w) and fluid attenuated inversion recovery (FLAIR) images, which occur predominantly in the white matter periventricular area. Other favored locations of MS plaques include the corpus callosum, the white matter around the temporal horns of the lateral ventricles, and the middle cerebellar peduncles [4,5].

Several pathologic conditions may produce similar MRI manifestations that can mimic MS, like cerebral microangiopathies (CM), which may produce T2-w or FLAIR hyperintensities resembling MS [6]. These hyperintensities

* Corresponding author. Medical Image Processing and Analysis (MIPA) Group, Department of Medical Physics, School of Medicine, University of Patras, 26500 Rio, Greece. Tel.: +302610997745.

E-mail address: theochar@upatras.gr (P. Theodorakis).

URL: <http://mipa.med.upatras.gr> (P. Theodorakis).

are produced from the occlusion of small arteries arising from the major cerebral arteries and produce white matter lesions, usually called “lacunar” infarcts, which are very common over the age of 50 [7,8]. The problem arises when the patient is middle aged; thus, the radiologist’s evaluation on MS-probable cases may become a complex task, whether to decide if it is an MS case, which remained asymptomatic (clinical silent) [9] and/or had very late onset [10], or a CM case that occurred earlier due to cerebrovascular risk factors such as hypertension and migraine [1].

Previous studies have attempted to differentiate MS from other diseases infecting the CNS, including CM, in a qualitative and quantitative manner. In the Bot et al. [11] study, brain and spinal cord images of 25 MS patients and 66 patients with other neurologic diseases (17 of 66 with cerebrovascular disease) were compared. Two observers have scored the images according to several diagnostic criteria [12–14] and have also categorized the lesions according to their location. Statistical analysis, such as Student’s *t* test and Mann–Whitney *U* test, was utilized in order to determine the value of MRI in differentiating MS from other neurologic disorders, including CM. The study concluded that spinal cord images were abnormal in 92% of MS patients in contrast with the 6% of the second group, leading to the conclusion that spinal MRI can help in the differentiation between MS and other diseases affecting the CNS. Miller et al. [15] compared the MR characteristics of patients with vasculitis, another differential diagnosis of MS, to MS radiological manifestations. The comparison was performed by categorizing and evaluating the shape, intensity and position of the lesions. Although certain MRI abnormalities had suggested vasculitis, there have been cases where extra clinical information was needed. Acute disseminated encephalomyelitis (ADEM), which may constitute differential diagnosis of MS, has been studied by Singh et al. [16]. The MR imaging features, such as size, site, morphology and pattern of brain and spinal cord involvement, matched with the clinical diagnosis in 78.6% of the cases with MS and in 78.9% of the cases with ADEM. In other studies, computer-based image analysis techniques have been performed for the characterization of the MS lesions appearing in MR images. Mathias et al. [17] have segmented regions of interest (ROIs) from spinal MR cross-sectional images of MS patients and from a normal control group. A total of eight texture features, four from the first-order statistics and four from the gray-level co-occurrence matrices (GLCM) [18], were extracted and the Student’s *t* test was used to evaluate the statistical difference between the features. The study has verified that significant statistical difference exists between normal control and MS patients. Yu et al. [19] performed textural feature analysis to discriminate active and nonactive MS lesions, and attained 88% and 96% sensitivity in correctly classifying active and nonactive lesions, respectively, by using linear discriminant analysis (LDA).

In this study, a pattern recognition system has been developed for the discrimination of MS from CM lesions based on texture analysis of MR images. Discrimination between MS and CM by employing textural features, to the best of our knowledge, has not been previously investigated. The proposed pattern recognition system was designed by utilizing the probabilistic neural network (PNN) classifier [20] evaluated using an external cross-validation (ECV) procedure [21]. Furthermore, the textural features that contributed the most in the ECV procedure were analyzed for statistically significant differences between MS and CM with the nonparametric Mann–Whitney *U* test. In this way, we could investigate the potentiality of MR textural features as a possible surrogate marker in differentiating MS from CM.

2. Methods

2.1. MR Images

The MS group included in this study comprised 11 patients diagnosed with clinically definite MS [3]. The mean age of the patients was 45 years old (mean age: 43.6 years; standard deviation: 8.1; range: 36–52 years) and the male-to-female ratio was 4:10. For each patient, two sets of 20 axial slices covering the entire brain were obtained at 1.5-T modality (MAGNETOM *Sonata*, Siemens, Erlangen, Germany) using the fluid attenuated inversion recovery protocol (TR: 9000 ms; TE: 117 ms; TI: 2500 ms; acquisition matrix: 320×208). Field of view was set at 230×230 mm with a 5-mm slice thickness and 1.5-mm space between two consecutive slices. The CM group consisted of 18 patients with a mean age of 54.3 years (S.D.: 12.8; range: 45–59 years); male-to-female ratio was 6:10, while seven were found with hypertension, four had diabetes and seven had high cholesterol combined with obesity. CM patients’ characterization was based on MRI evaluation and patient clinical information. Fig. 1 illustrates the axial FLAIR image of a 43-year-old male with MS and a 51-year-old male with CM.

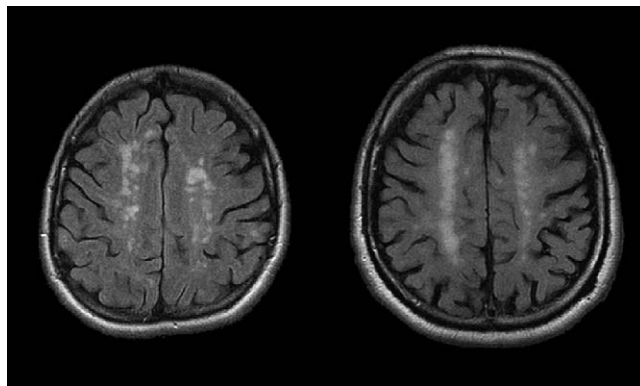


Fig. 1. Axial FLAIR images from a 43-year-old male with MS (left) and from a 51-year-old male with CM (right).

2.2. Region of interest and feature extraction

Three expert radiologists (KT, MM and GD) and a radiographer (KS) were asked to specify in consensus ROIs which included MS or CM lesions, resulting in 47 CM and 31 MS ROIs, using a custom-developed software. The criteria regarding the ROI selection were as follows: (1) from each lesion only one ROI was selected, (2) each selected ROI was through the slice with the largest lesion diameter, (3) only lesions larger than 5 mm in diameter were used and (4) clustered lesions in a patient were excluded (i.e., only singular lesions were considered). From each ROI, a series of 23 textural features were extracted, four features from the ROI's histogram, 14 from the co-occurrence matrices (GLCM) [18] and five from the run-length matrices [22]. All features were normalized to zero mean and unit standard deviation [23], according to Eq. (1)

$$x'_i = \frac{x_i - m}{\text{std}} \quad (1)$$

where x_i and x'_i are the i th feature values before and after the normalization, respectively, and m and std are the mean value and standard deviation, respectively, of feature x_i over all features and both groups (classes).

2.3. Pattern recognition scheme and statistics

The whole image analysis work was based on processing and analysis of image ROIs. In order to evaluate the discriminatory power of the textural features calculated from MS and CM ROIs, the minimum distance (MD) [23], the LDA [24], the logistic regression (LR) [24] and the PNN [20] classifiers were employed.

A description of the PNN is given below, since it was adopted for the design of the system. The PNN is a nonparametric feed-forward neural network classifier with the discriminant function given in Eq. (2).

$$g_i(\mathbf{x}) = \frac{1}{(2\pi)^{d/2} \sigma^d N_i} \sum_{j=1}^{N_i} \exp \left[-\frac{(\mathbf{x} - \mathbf{x}_{ij})^T (\mathbf{x} - \mathbf{x}_{ij})}{2\sigma^2} \right] \quad (2)$$

The feature vector to be classified is \mathbf{x} , \mathbf{x}_{ij} is the training feature vector (a number of appropriately selected features representing each ROI) used to design the PNN classifier, σ is the spread of the Gaussian activation function, N_i is the number of training feature vectors (or patterns) in class i and d is the dimensionality of the feature vectors.

Subsequently, since the leave-one-out method has been proven to provoke optimistically biased estimates of the classifier's performance, the accuracy of the PNN classifier was evaluated using an ECV process for more reliable estimates as described in Ref. [21]. According to the ECV, the data were randomly split into two main subsets: a training subset comprising two thirds (52 feature vectors) of available ROI samples (training data) and a test subset consisting of the remaining one third (26 feature vectors) of available ROI

samples (test data). The training data were used for feature selection and for training of the PNN classifier using the exhaustive search and the leave-one-out methods [23]. Following feature selection and PNN design, the performance of the PNN classifier was then evaluated on the remaining test data. In this way, the dataset involved in the selection of best features and the dataset used in the evaluation differed; thus, any bias was avoided. This process was repeated 10 times for 10 different random splits of all available samples into training and test data. The average accuracies were computed. In this way, the ECV estimate of the classifiers' performance was determined. ECV provides one of the most unbiased estimators of the generalization error, and in order to mark out this attribute, the system was also validated without the ECV but employing the leave-one-out method alone.

The features that contributed the most in the ECV were checked for significant differences by the Mann–Whitney U test [25]. In this way, the existence of any statistically significant differences was evaluated in order to be able to assess textural differences between MS and CM, and probably account for their contribution in the differential diagnosis of MS from CM.

3. Results

With the use of the leave-one-out method, best overall accuracy (88.46%) in discriminating MS from CM lesions was attained by the PNN classifier. The rate of correct identification was 87.09% (27/31) for MS lesions and 89.36% (42/47) for CM lesions. The LDA, MD and LR classifiers resulted in inferior performances as can be seen in Table 1. Specific (MS and CM) and overall classification accuracies for all classifiers are shown in Fig. 2. Considering patient classification, 9 of 11 MS cases and 14 of 18 CM cases were correctly classified, where correct case classification was considered only if all ROIs of the case were correctly classified. Employing the correlation coefficient, we found that between image ROIs of the same

Table 1
Results using the LDA, MD, LR and PNN classifiers

		MS	CM	Accuracy (%)	
LDA	Best features: sum of entropy,	MS	24	7	77.41
	difference of variance	CM	6	41	87.23
	Overall accuracy				83.33
MD	Best features: sum of variance,	MS	25	6	80.64
	S.D.	CM	6	41	87.23
	Overall accuracy				84.61
LR	Best features: sum of variance,	MS	22	9	70.96
	entropy, inverse moment correlation	CM	4	43	91.48
	Overall accuracy				83.33
PNN	Best features: mean value,	MS	27	4	87.09
	sum of variance, run	CM	5	42	89.36
	length nonuniformity				88.46
	Overall accuracy				88.46

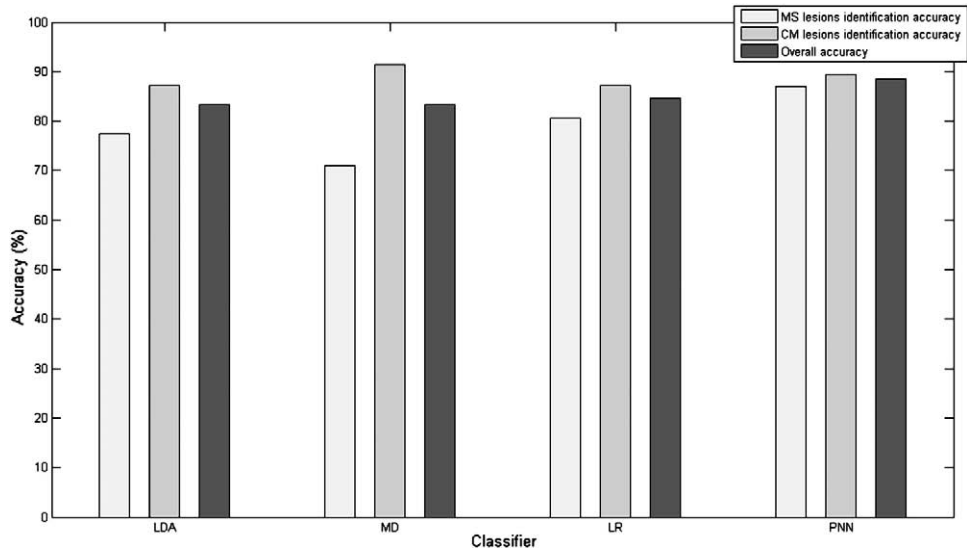


Fig. 2. Specific (MS and CM) and overall classification accuracies for all classifiers employed using the leave-one-out method.

patient, correlations varied between 0.02 and 0.3. This indicates that image ROIs in each one of the patient had none or very low textural resemblance. Fig. 3 depicts the scatter diagram of the best features used to design the PNN classifier and its decision boundary. With the use of the ECV method, the mean accuracy for the PNN classifier was 72.96%. In Table 2, the frequency of occurrence of each feature in the 10 repetitions of the ECV, together with the features' mean values and the standard deviations (in parentheses), is presented. The most frequently occurring features were the mean value, contrast, sum of average and sum of variance. Table 3 presents the results of the Mann–Whitney *U* test for determining the discriminatory

capability of each feature. The statistical threshold value was set at $P=0.05$. Accordingly, all features, but skewness and gray level nonuniformity ($P>0.05$), were found to be statistically plausible to discriminate MS from CM lesions. Table 4 provides information about the ROIs' width, height (in millimeters and pixels) and total area in square millimeters.

4. Discussion

Differentiating on MRI between MS and CM can be a complex task, since MRI features are often indistinguish-

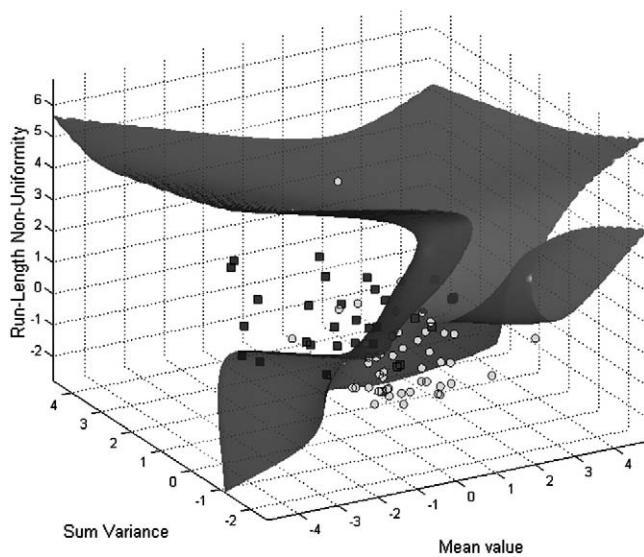


Fig. 3. Scatter diagram of the best features used to design the PNN classifier and its decision boundary.

Table 2

Frequencies of occurrence, mean values and the standard deviations of textural features employed in the ECV procedure

Feature	Occurrence	CM Mean (S.D.)	MS Mean (S.D.)
Mean	4	128.861 (16.557)	118.246 (21.105)
Contrast	3	12.225 (7.979)	29.016 (16.656)
Sum of average	3	114.888 (4.568)	107.332 (4.776)
Sum of variance	3	49.261 (46.947)	140.805 (83.845)
Angular second moment	2	0.026 (0.012)	0.014 (0.005)
Correlation	2	0.503 (0.203)	0.623 (0.136)
Inverse different moment	2	0.329 (0.081)	0.234 (0.045)
IMC2	2	0.884 (0.074)	0.951 (0.035)
Gray level nonuniformity	2	6.418 (3.317)	5.040 (2.052)
Run-length nonuniformity	2	53.632 (30.991)	71.561 (25.628)
Skewness	1	-0.622 (0.440)	-0.587 (0.493)
Sum of entropy	1	2.794 (0.369)	3.272 (0.273)
Entropy	1	3.934 (0.463)	4.489 (0.332)
Difference variance	1	4.616 (3.316)	11.080 (7.415)
Run percentage	1	0.102 (0.024)	0.114 (0.021)

Table 3
Statistical analysis of the contributing features (significance level set at $P=.05$)

Feature	U value	z Value	P value	Significant difference
Mean	974	2.506	.012	Yes
Skewness	777	0.495	.620	No
Angular second moment	1245	5.273	1.34E-07	Yes
Contrast	1263	5.457	4.83E-08	Yes
Correlation	982	2.588	.009	Yes
Inverse different moment	1252	5.345	9.03E-08	Yes
Sum of average	1283	5.661	1.50E-08	Yes
Sum of variance	1248	5.304	1.13E-07	Yes
Sum of entropy	1243	5.253	1.49E-07	Yes
Entropy	1221	5.028	4.94E-07	Yes
Difference of variance	1251	5.334	9.56E-08	Yes
IMC2	1186	4.671	2.99E-06	Yes
Gray-level nonuniformity	917	1.924	.0544	No
Run-length nonuniformity	1060	3.384	.0007	Yes
Run percentage	970	2.465	.013	Yes

able and management of patients with MS differs from that followed in patients with CM [5,26]. Additionally, employment of textural features on MRI has been previously used in differentiating between MS patients and normal controls [17] and between patients with active and nonactive MS lesions [19]. Results obtained have indicated existing textural differences, and their findings are comparable in accuracy to ours. They have found classification accuracies of 96% for nonactive and 88% for active MS lesions, while in our study best classification accuracy for nonactive MS lesions was about 87.09% as shown in Table 1. However, it has to be pointed out that the results in Ref. [19] have been obtained using different classification algorithms to ours and discrimination accuracies in the said study [19] were achieved by differentiating partly different types of lesions to ours (active MS vs. non active MS against nonactive MS vs. CM lesions, respectively).

In most previous studies [11,15,16], assessment of MS lesions' nature and corresponding differential diagnosis have been performed by visual evaluation of the lesion's features such as size, site, morphology and spinal cord involvement. Only in Ref. [17] has an attempt been made to assess the lesion's texture by computer methods. Such analysis may be of value since pixel values, pixel interrelations and lesion texture may be more accurately analyzed by computer methods than they can be visually estimated. According to the findings of the present study, there exist significant differences in the values of the textural features between CM and MS (Table 3).

Those textural features might encode meaningful interpretations regarding the clinical context of MS and CM. The mean value is an index that intuitively shows the brightness of each ROI. As can be seen from Table 2, MS ROIs are less bright than CM ROIs. Another important textural feature is contrast, which is a measure of local variation between pixel intensities. MS regions had higher contrast values than CM regions. Angular second moment (ASM) and inverse different moment (IDF) are both related to ROI's homogeneity [18]. In CM regions, ASM and IDF had higher values than in MS regions, implying that CM regions were smoother (more homogeneous). From another perspective, MS ROIs attained higher entropy and sum of entropy values than CM ROIs, indicating that the degree of randomness of pixel intensities or textural roughness in MS regions was higher. Conclusively, MS regions were darker, of higher contrast, less homogeneous and rougher as compared to CM. These findings are in agreement with observations by Mathias et al. [17] regarding MS lesions. The latter were found with increased entropy and decreased angular second moment, implying that MS lesion texture was rough and of low homogeneity. This loss of homogeneity in MS may be attributed to a number of processes such gliosis, inflammation, demyelination and changes in water content that may disrupt MR signal intensity uniformity [17].

The computer-based approach we followed consisted of a PNN classifier and the ECV method for eliminating bias in the classifier's performance [21]. For the selection of the PNN, we followed a trial-and-error procedure, whereby the commonly employed MD, LDA and LR classifiers were first tested, since they are "standard textbook" techniques in many pattern-recognition applications [23]. Moreover, the LDA classifier has also been used for MS texture analysis on MR images in a previous study [19]. By applying those classifiers on the same dataset of the present study, it was found that their classification accuracies (84.61%, 83.33%, 83.33%, respectively) were lower than that of the PNN (88.46%), employing for comparative evaluation purposes the leave-one-out and exhaustive search methods (see Table 1). Fig. 3 shows a 3-D scatter diagram and the PNN's decision boundary for the best textural features used. As it may be seen, depicted points represent specific lesions and form two clusters corresponding to the MS (square points) and CM (circular points) classes. These classes are adequately separated by the PNNs' nonlinear surface. Additionally, as can be observed from Table 1 and Fig. 2 regarding specific (MS and CM) and overall classification accuracies, the PNN,

Table 4
MS and CM ROI sizes: mean value (S.D.)

	Width		Height		Area
	In pixels	In millimeters	In pixels	In millimeters	Square millimeters
MS	13.546 (2.276)	9.736 (1.636)	11.226 (2.880)	8.069 (2.070)	52.794 (17.681)
CM	12.334 (1.974)	8.865 (1.419)	14.653 (3.322)	10.532 (2.388)	44.328 (18.456)

despite being more accurate, seems to be more balanced regarding the specific MS and CM precisions, revealing only about 2% specific precision discrepancy against about 7% for the MD, 10% for the LDA and 19% for the LR classifiers. This additional observation has led us to choose the PNN for further analysis, i.e., employment of the ECV evaluation method. Additionally, as can be seen from Table 1 and the best textural features combination adopted by the classifiers, there are some features that appear in more than one classifier. This may indicate the importance of textural properties that they may convey such as the entropy- (entropy and sum of entropy) and variance- (difference of variance and sum of variance) based features. Additionally, this finding is in line with the significant statistical difference of those features shown in Table 3, employing the Mann–Whitney *U* test.

The above-obtained classification accuracies suffer from bias due to the fact that the dataset used for determining the best feature combination for a classifier is also involved in the performance evaluation of the classifier [21]. To demonstrate the degree of bias that may contaminate findings, the system's overall accuracy was falsely elevated to 88.46% against 72.96% when the ECV evaluation method was employed. Thus, ECV had to be used for estimating the performance of the proposed system to unseen data and thus for concluding on its reliability, if it were to be adopted as a second opinion tool in discriminating MS from CM.

In conclusion, textural features may encapsulate properties for characterizing MS and CM lesions. The presented system can be used as a second opinion tool for assisting the radiologist, when MS vs. CM differential diagnosis problem arises, which is critical for the patient's management.

Acknowledgments

We would like to thank the Greek State Scholarship Foundation (IKY) for funding this work.

References

- [1] Ropper AH, Brown RH. Adams and Victor's principles of neurology. New York: McGraw-Hill; 2005.
- [2] Olek MJ. Multiple Sclerosis Etiology, Diagnosis, and new Treatment Strategies. Totowa (NJ): Humana Press; 2005.
- [3] McDonald WI, Compston A, Edan G, Goodkin D, Hartung HP, Lublin FD, et al. Recommended diagnostic criteria for multiple sclerosis: guidelines from the International Panel on the diagnosis of multiple sclerosis. *Ann Neurol* 2001;50:121–7.
- [4] Pretorius PM, Quaghebeur G. The role of MRI in the diagnosis of MS. *Clin Radiol* 2003;58:434–48.
- [5] Cook SD. Handbook of Multiple Sclerosis. London: Taylor & Francis; 2006.
- [6] Fadiel H, Kelley RE, Gonzalez-Toledo E. Differential diagnosis of multiple sclerosis. *Int Rev Neurobiol* 2007;79:393–422.
- [7] Ringelstein EB, Nabavi DG. Cerebral small vessel diseases: cerebral microangiopathies. *Curr Opin Neurol* 2005;18:179–88.
- [8] Schmidtke K, Hull M. Cerebral small vessel disease: how does it progress? *J Neurol Sci* 2005;229-230:13–20.
- [9] Heinsen H, Lockemann U, Puschel K. Unsuspected (clinically silent) multiple sclerosis. Quantitative investigations in one autoptic case. *Int J Legal Med* 1995;107:263–6.
- [10] Azzimondi G, Stracciari A, Rinaldi R, D'Alessandro R, Pazzaglia P. Multiple sclerosis with very late onset: report of six cases and review of the literature. *Eur Neurol* 1994;34:332–6.
- [11] Bot JC, Barkhof F, Lycklama a Nijeholt G, van Schaardenburg D, Voskuyl AE, Ader HJ, et al. Differentiation of multiple sclerosis from other inflammatory disorders and cerebrovascular disease: value of spinal MR imaging. *Radiology* 2002;223:46–56.
- [12] Barkhof F, Filippi M, Miller D, Scheltens P, Campi A, Polman C, et al. Comparison of MRI criteria at first presentation to predict conversion to clinically definite multiple sclerosis. *Brain* 1997;120:2059–69.
- [13] Fazekas F, Offenbacher H, Fuchs S, Schmidt R, Niederkorn K, Horner S, et al. Criteria for an increased specificity of MRI interpretation in elderly subjects with suspected multiple sclerosis. *Neurology* 1988;38:1822–5.
- [14] Paty DW, Oger JJ, Kastrukoff LF, Hashimoto SA, Hooze JP, Eisen AA, et al. MRI in the diagnosis of MS: a prospective study with comparison of clinical evaluation, evoked potentials, oligoclonal banding, and CT. *Neurology* 1988;38:180–5.
- [15] Miller DH, Ormerod IE, Gibson A, du Boulay EP, Rudge P, McDonald WI. MR brain scanning in patients with vasculitis: differentiation from multiple sclerosis. *Neuroradiology* 1987;29:226–31.
- [16] Singh S, Prabhakar S, Korah IP, Warade SS, Alexander M. Acute disseminated encephalomyelitis and multiple sclerosis: magnetic resonance imaging differentiation. *Australas Radiol* 2000;44:404–11.
- [17] Mathias JM, Tofts PS, Losseff NA. Texture analysis of spinal cord pathology in multiple sclerosis. *Magn Reson Med* 1999;42:929–35.
- [18] Haralick RM, Shanmugam K, Dinstein I. Textural Features for image classification. *IEEE Trans Syst Man Cybern SMC* 1973;3:610–21.
- [19] Yu O, Mauss Y, Zollner G, Namer IJ, Chambron J. Distinct patterns of active and non-active plaques using texture analysis on brain NMR images in multiple sclerosis patients: preliminary results. *Magn Reson Imaging* 1999;17:1261–7.
- [20] Specht DF. Probabilistic neural networks. *Neural Networks* 1990;3:109–18.
- [21] Ambrose C, McLachlan GJ. Selection bias in gene extraction on the basis of microarray gene-expression data. *Proc Natl Acad Sci* 2002;99:6562–6.
- [22] Galloway MM. Texture analysis using grey level run lengths. *Comp Graph Image Proc* 1975;4:172–9.
- [23] Theodoridis S, Koutroumbas K. Pattern Recognition. UK: Academic Press; 1998. p. 25, 165, 388.
- [24] Krzanowski WJ. Principles of Multivariate Analysis: A User's Perspective. New York: Oxford University Press; 2000.
- [25] Conover WJ. Practical Non Parametric Statistics. Wiley; 1998.
- [26] Adams PH, Hachinski V, Norris JW. Ischemic Cerebrovascular Disease. New York: Oxford University Press; 2001.